Journal of Controlled Release 367 (2024) 327–338

Contents lists available at ScienceDirect

Journal of Controlled Release

journal homepage: www.elsevier.com/locate/jconrel

Backbone cationized highly branched poly(β-amino ester)s as enhanced delivery vectors in non-viral gene therapy

Yinghao Li [a,b,1], Bei Qiu [b,1], Zishan Li [b], Xianqing Wang [b], Zhonglei He [a], Darío Manzanares Sandoval [b], Rijian Song [b], A. Sigen [c], Chunyu Zhao [b], Melissa Johnson [b], Jing Lyu [b,*], Irene Lara-Sáez [b,*], Wenxin Wang [a,b,*]

[a] Institute of Precision Medicine (AUST-IPM), Anhui University of Science and Technology, Huainan 232001, China
[b] Charles Institute of Dermatology, School of Medicine, University College Dublin, D04 V1W8 Dublin, Ireland.
[c] School of Medicine, Anhui University of Science and Technology, Huainan 232001, China

ARTICLE INFO

Keywords:
Non-viral gene delivery
Poly(β-amino ester)
Backbone cationization
Highly branched structure
Cystic fibrosis

ABSTRACT

Gene therapy holds great potential for treating Lung Cystic Fibrosis (CF) which is a fatal hereditary condition arising from mutations in the CF transmembrane conductance regulator (CFTR) gene, resulting in dysfunctional CFTR protein. However, the advancement and clinical application of CF gene therapy systems have been hindered due to the absence of a highly efficient delivery vector. In this work, we introduce a new generation of highly branched poly(β-amino ester) (HPAE) gene delivery vectors for CF treatment. Building upon the classical chemical composition of HPAE, a novel backbone cationization strategy was developed to incorporate additional functional amine groups into HPAE without altering their branching degree. By carefully adjusting the type, proportion, and backbone distribution of the added cationic groups, a series of highly effective HPAE gene delivery vectors were successfully constructed for CF disease gene therapy. In vitro assessment results showed that the backbone cationized HPAEs with randomly distributed 10% proportion of 1-(3-aminopropyl)-4-methylpiperazine (E7) amine groups exhibited superior transfection performance than their counterparts. Furthermore, the top-performed backbone cationized HPAEs, when loaded with therapeutic plasmids, successfully reinstated CFTR protein expression in the CFBE41o- disease model, achieving levels 20–23 times higher than that of normal human bronchial epithelial (HBE) cells. Their therapeutic effectiveness significantly surpassed that of the currently advanced commercial vectors, Xfect and Lipofectamine 3000.

1. Introduction

Cystic fibrosis (CF), a hereditary and life-threatening condition resulting from mutations in the CF transmembrane conductance regulator (CFTR) gene, affects over 100,000 individuals globally. [1,2] The primary cause of morbidity and mortality is progressive lung disease, making the lung a critical target for therapeutic intervention. With over 2000 mutations in the CFTR gene, the prevalent Phe508del mutation leads to a malfunctioning CFTR protein, causing airway mucus dehydration, pH alterations, recurrent infections, inflammation, and pulmonary failure. [3] While medications offer symptom relief, they do not provide a cure. [4] The recent advancements in the field include the use of CFTR modulators, which include correctors and potentiators like elexacaftor, ivacaftor, tezacaftor, and lumicaftor. [5–7] These treatments focus on rectifying the malfunctioning protein, but they do not benefit all patients. Gene replacement emerges as a promising strategy, capable of generating functional CFTR protein in the lung, offering the potential for addressing diverse mutation types. [8,9] However, advancements in gene therapy systems for CF are impeded by the absence of highly efficient delivery vectors. Traditional viral vectors, exemplified by adenovirus (Ad), elicit immune responses within the therapeutic context. [10] Furthermore, adeno-associated viruses (AAV) present limited packaging capacity, leading to diminished CFTR expression levels. [9] Conversely, non-viral vectors offer advantages in ease of modification and decoration, presenting solutions to challenges linked with inflammation and immune responses, rendering them more auspicious candidates for constructing safe and effective therapeutic systems. [11–13]

* Corresponding authors.
E-mail addresses: jing.lyu@ucd.ie (J. Lyu), wenxin.wang@ucd.ie (W. Wang).
[1] These authors contributed to this work equally.

https://doi.org/10.1016/j.jconrel.2024.01.046
Received 28 November 2023; Received in revised form 19 January 2024; Accepted 22 January 2024
Available online 1 February 2024

Within the realm of non-viral vectors, cationic lipid and polymer vectors take precedence. Although lipid-based vectors have historically dominated the development of non-viral therapeutic systems for CF, they have fallen short of meeting clinical requirements, often causing inflammation and cytotoxicity. [14–16] In contrast, non-viral polymeric vectors coupled with demonstrated high transfection efficiency and low cytotoxicity make them highly appealing candidates for CF therapeutic system development. [11,17–19] Among the myriad polymeric carriers, poly(β-amino esters) (PAEs) stand out as star candidates for constructing effective CF gene therapy systems, offering advantages of high cell viability, a substantial genetic payload capacity, inexpensive synthesis, facile purification, and scalability. [20–25] Linear PAE (LPAE), initially developed by Lynn and Langer in 2000, [26] has since seen the creation of thousands of LPAE vectors utilized in diverse genetic disease studies and clinical trials. [27–29] While LPAEs have shown encouraging results, their linear nature inherently limits the synthesis and optimization of structures with multiple functional groups. In 2016, Wang et al. [25] introduced a significant advancement by constructing highly branched PAEs (HPAEs) through a straightforward A2 + B3 + C2 Michael addition strategy. The transition from linear to branched structures introduced numerous terminal functional groups, considerably enhancing interactions with DNA, improving the formation of polymer/DNA polyplexes, protecting the encapsulated DNA from degradation, and increasing the cellular uptake of polymer/DNA polyplexes. [30,31] Consequently, the HPAE gene transfection performance significantly improved compared to their linear counterparts. [25,32,33]

Given the obvious potential of HPAE in gene transfection, it is hugely appealing to exploit its performance in CF gene therapy. Therefore, in this work, we further optimized the HPAE structure and evaluated their potential in CF disease treatment. First, given that the improved performance of HPAE is attributed to the introduction of more cationic terminal groups compared to LPAE, which play a crucial role in processes like DNA compression, cell recognition, cellular uptake, and endosomal escape, as demonstrated in previous studies. [25,32,33] Therefore, based upon a proven efficient HPAE monomer set, a novel backbone cationization strategy was proposed to further enhance the HPAE gene transfection performance while maintaining their highly branched topology and branching degree. A series of HPAEs with additional cationic moieties incorporated into the polymer backbone were synthesized and applied to CFTR gene transfection in CFBE41o- disease model. The top-performed backbone cationized HPAE vectors were screened out by optimizing the type, proportion, and distribution of the newly introduced cationic moieties, respectively. They were further loaded with therapeutic plasmids to reinstate CFTR protein expression in the CFBE41o- disease model, and the results were compared with the performance of the commercial vectors, Xfect and Lipofectamine 3000.

2. Materials and methods

2.1. Synthesis of PAEs

For HP1-A to —F synthesis, monomers 1,4-butanediol diacrylate (BDA), 5-amino-1-pentanol (S5), pentaerythritol tetraacrylate (PTTA) and different tertiary amines [1-(3-aminopropyl)-4-methylpiperazine (A/E7), 3-Morpholinopropylamine (B), 3-(Dimethylamino)-1-propylamine (C), 1-(3-Aminopropyl)imidazole (D), 3-(Diethylamino)propylamine (E), 4-Aminobutyraldehyde diethyl acetal (F) (see feed ratios in **Table S1**) were dissolved in dimethyl sulfoxide (DMSO) at the concentration of 30% *w/v*. The reaction occurred under argon protection. Once the polymer reached the desired molecular weight, the end-capping amines, E7, were added to stop the reaction, and the reaction system was diluted to 10% *w/v* (**Fig. S1** to **S6**). In the end, the polymers were precipitated into diethyl ether for purification and were dried under vacuum.

For HP2-A to —F synthesis, monomers 1,4-butanediol diacrylate (BDA), 5-amino-1-pentanol (S5), PTTA and different amount of E7 (see feed ratios in **Table S2**) were dissolved in dimethyl sulfoxide (DMSO) at the concentration of 30% *w/v*. The reaction occurred under argon protection. Once the polymer reached the desired molecular weight, the end-capping amines (E7), were added to stop the reaction, and the reaction system was diluted to 10% *w/v* (**Fig. S7** to **S11**). In the end, the polymers were precipitated into diethyl ether for purification and were dried under vacuum.

For HP3-A synthesis. The same as HP2-C (**Table S3**), monomers BDA, S5, PTTA, and E7 were dissolved in DMSO at the concentration of 30% *w/v*. The reaction occurred under argon protection. Once the polymer reached the desired molecular weight, the end-capping amines (E7), were added to stop the reaction, and the reaction system was diluted to 10% *w/v*. In the end, the polymers were precipitated into diethyl ether for purification and were dried under vacuum.

For HP3-B synthesis (**Table S3**). Monomers BDA, S5, and PTTA were dissolved in DMSO at the concentration of 30% *w/v*. The reaction was conducted until the molecular weight reached 5 kDa (Step 1, **Fig. S12**). BDA and E7 were dissolved in DMSO and polymerized until the molecular weight reached 1 kDa (Step 2, **Fig. S13**). Then the products of Step 1 and Step 2 were mixed. The reaction was further conducted until the molecular weight of the polymers reached 8 kDa (Step 3, **Fig. S14**). The end-capping amines (E7), were added to stop the reaction, and the reaction system was diluted to 10% *w/v*. In the end, the polymers were precipitated into diethyl ether for purification and were dried under vacuum.

For HP3-C synthesis (**Table S3**). Monomers BDA, and E7 were dissolved in DMSO at the concentration of 30% *w/v*. The reaction was conducted until the molecular weight reached 1.5 kDa (Step 1, **Fig. S15**). The rest of the monomers (BDA, S5, PTTA) were added into the system and polymerized until the molecular weight of the polymer reached 8 kDa (Step 2, **Fig. S16**). The end-capping amines (E7), were added to stop the reaction, and the reaction system was diluted to 10% *w/v*. In the end, the polymers were precipitated into diethyl ether for purification and were dried under vacuum.

For HP3-D synthesis (**Table S3**). monomers E7, and PTTA were dissolved in DMSO at the concentration of 30% *w/v*. The reaction was conducted until the molecular weight reached 0.9 kDa (Step 1, **Fig. S17**). BDA and S5 were dissolved in DMSO and polymerized until the molecular weight reach 1.5 kDa (Step 2, **Fig. S18**). Then the products of Step 1 and Step 2 were mixed. The reaction was further conducted until the molecular weight of the polymer reached 8 kDa (Step 3, **Fig. S19**). The end-capping amines (E7), were added to stop the reaction, and the reaction system was diluted to 10% *w/v*. In the end, the polymers were precipitated into diethyl ether for purification and were dried under vacuum.

For HP3-E synthesis (**Table S3**). Monomers E7 and PTTA were dissolved in DMSO at the concentration of 30% *w/v*. The reaction was conducted until the molecular weight reached 1.2 kDa (Step 1, **Fig. S20**). The rest of the monomers (BDA, S5, PTTA) were added into the system and polymerized until the molecular weight of polymer reached 8 kDa (Step 2, **Fig. S21**). The end-capping amines (E7), were added to stop the reaction, and the reaction system was diluted to 10% *w/v*. In the end, the polymers were precipitated into diethyl ether for purification and were dried under vacuum.

Gel Permeation Chromatography (GPC) was used to monitor the reaction and characterize the molecular weights, polydispersity and Mark-Houwink Index. ^{1}H Nuclear Magnetic Resonance (NMR) was used to confirm the chemical structures of HPAEs. All the reagents mentioned above were purchased from Merck (Rahway, NJ, USA).

2.2. Molecular weight and dispersity measurements

Number average molecular weight (M_n), weight average molecular weight (M_w), Mark−Houwink (MH) and dispersity ($Đ$) of polymers were determined by GPC equipped with a refractive index detector (RI), a

viscometer detector (VS DP) and a dual angle light scattering detector (LS 15° and LS 90°). To test the molecular weight of polymers during the polymerization process, 20 μl of the reaction mixture was collected at different time points, and diluted with 1 ml of DMF, then filtered through a 0.2 μm filter, and then measured by GPC. The columns (PolarGel-M, Edinburgh, UK, 7.5 mm × 300 mm, two in series) were eluted with DMF and 0.1% LiBr at a flow rate of 1 ml/min at 60 °C. Columns were calibrated with linear poly(methyl methacrylate) (PMMA) standards.

2.3. Nuclear magnetic resonance (NMR)

The chemical structure and composition of polymers were confirmed with ^{1}H NMR. Polymer samples were dissolved in $CDCl_3$. Measurements were carried out on a Varian Inova 400 MHz spectrometer.

2.4. Cell culture

CFBE41o- human CF bronchial epithelial and 16HBE14o- human bronchial epithelial cell lines were derived from a CF patient homozygous for the Phe508del CFTR mutation and a healthy donor, respectively, and both were immortalized with the origin-of-replication defective SV40 plasmid (pSVori-) (Merck). Cells were grown in flasks or plates coated with a Fibronectin/Collagen/BSA extracellular matrix cocktail (Merck) in Minimum Essential Medium (MEM) cell culture medium (Merck) supplemented with 10% fetal bovine serum (FBS) (Thermo Fisher Scientific), 1× MEM Non-essential amino acid (only for CFBE41o- cell culture) (Merck), 2 mM glutamine (Thermo Fisher Scientific) and 100 U/ml penicillin, 100 μg/ml streptomycin sulphate (Thermo Fisher Scientific). A549 human lung cancer cells were derived from the lung tissue from the patient with lung cancer. Cells were grown in flasks or plates in Dulbecco's Modified Eagle Medium (DMEM) cell culture medium (Merck) supplemented with 10% FBS and 100 U/ml penicillin, 100 μg/ml streptomycin sulphate. All the cells were incubated at 5% CO_2 at 37 °C.

2.5. Cell transfection

Cells were seeded approximately 24 h in advance at a density of around 20,000 cells per square centimeter. Transfections were conducted when the cell confluence reached 50%–70%. The transfection process involved introducing a series of HPAE polymers, which were designed and synthesized by our research group, or commercial transfection reagents, namely Lipofectamine™ 3000 from Thermo Fisher Scientific, Xfect™ from Takara, Kusatsu, Japan, and BrB203 from Branca Bunús, Dublin, Ireland. The transfection took place in the culture medium, with plasmids at a final concentration of 5 ng/μl, previously complexed with the various synthesized polymers. The polymers and DNA were diluted in 25 mM Sodium Acetate (NaAc) at weight-to-weight (*w*/w) ratios of 10:1 and 20:1, then mixed at a 1:1 volume-to-volume (*v*/v) ratio. The expression of the reporter gene green fluorescent protein (GFP) was observed 48 h post-transfection using an Olympus IX81 fluorescence microscope (Olympus, Tokyo, Japan). The intensity of GFP fluorescence was analyzed and semi-quantified using ImageJ software (NIH, Bethesda, MD, USA).

2.6. Cell viability

AlamarBlue™ Kit (Thermo Fisher Scientific) was used to assess the cell viability. The method has been previously described. In brief, the cell viability was tested 48 h post-transfection by replacing the previous medium with fresh medium containing 10% (*v*/v) alamarBlue™ reagent. A SpectraMax M3 multi-plate reader (Molecular Devices, San Jose, CA, USA) was used for Excitation/Emission values determination, which was recorded at 570 nm and 590 nm after incubating cells with 10% alamarBlue™ for 2 h protected from light at 37 °C. The untreated cells were used to normalize fluorescence values and set as 100% cell viability.

2.7. Cellular uptake of polyplexes

The Cy3 DNA labeling kit from Mirus (Marietta, GA, USA) was employed for DNA labelling, following the manufacturer's instructions. CFBE14o- cells were transfected with HPAE3/DNA polyplexes (weight-to-weight ratio, *w*/w = 20:1), Lipofectamine3000/DNA lipoplexes, and Xfect/DNA polyplexes using 5 ng/μl of DNA. The transfection process lasted for 4 h, after which the cells were incubated with NucBlue™ Live Ready Probes™ Reagent from Thermo Fisher Scientific at room temperature for 30 min. Fluorescent images were captured using an Olympus IX81 fluorescence microscope.

2.8. DNA binding assay

The DNA binding capacity of each polymer was quantified using Quant-iT™ PicoGreen™ dsDNA Assay Kits from Thermo Fisher Scientific. Polyplexes, prepared with the same formulation as cell transfection, were combined with PicoGreen working solution and incubated for 5 min. Fluorescence was measured with a SpectraMax M3 plate reader. DNA binding efficiency (BE) was calculated using the formula: $BE = ((F_{DNA}\text{-}F_{Sample})/(F_{DNA}\text{-}F_{Blank})) \times 100\%$, where F_{DNA} is the fluorescence of free DNA, F_{Sample} is the fluorescence of a polyplex, and F_{Blank} is the fluorescence from PicoGreen working solution with the buffer used for polyplex or lipoplex formulation.

2.9. Polyplex size and zeta potential

The size zeta potential of polyplexes or lipoplexes, formed by combining the polymer or lipid with DNA (gWiz-GFP or CpG-deplete CFTR plasmids), was assessed using a Zetasizer Pro (Malvern Panalytical, Malvern, UK). Following the previously outlined preparation method, the polyplexes or lipoplexes were diluted to 1 ml using their respective transfection buffers for measurement. The sample temperature was maintained at 25 °C during the analysis.

2.10. Western blot analysis

At 48 h post-transfection, cells were rinsed with DPBS (Thermo Fisher Scientific), followed by the addition of radioimmunoprecipitation assay (RIPA) buffer (Thermo Fisher Scientific) containing protease inhibitor (Thermo Fisher Scientific) to lyse the cells and solubilize proteins. Protein quantification was conducted using the Pierce BCA Protein Assay Kit (Thermo Fisher Scientific). Subsequently, samples were loaded onto 7% NuPAGE Tris-Acetate protein gels (Thermo Fisher Scientific) and transferred to a nitrocellulose membrane (Thermo Fisher Scientific). For CFTR protein detection, the primary antibody, mouse anti-human CFTR UNC-596 (University of North Carolina, NC, USA), was diluted at 1:500, and the secondary antibody, anti-mouse IgG, HRP-linked (Cell Signaling, Danvers, MA, USA), was diluted at 1:2000. Human α-tubulin (Cell Signaling) served as the loading control protein at a dilution of 1:1000, with the secondary anti-rabbit IgG, HRP-linked antibody (Cell Signaling), diluted at 1:4000. Protein bands were visualized and captured using Pierce™ ECL Western Blotting Substrate (Thermo Fisher Scientific) and the iBright CL750 Imaging System (Thermo Fisher Scientific). Semi-quantitative analysis of CFTR was performed using ImageJ Fiji software (NIH).

2.11. Immunocytochemistry analysis

After three washes with DPBS, both treated and untreated cells underwent fixation in 4% paraformaldehyde (Thermo Fisher Scientific) and permeabilization with 0.5% Triton X-100 (Merck). Subsequently, cells were blocked using 3% BSA (Merck). For CFTR protein detection,

the primary antibody, mouse anti-human CFTR UNC-570 (University of North Carolina, NC, USA), was diluted at 1:200. The secondary antibody, AlexaFluor™568-labeled goat anti-Mouse IgG (H + L) (Thermo Fisher Scientific), was diluted at 1:800. Nuclei were stained with DAPI (Abcam), and images were captured using an Olympus IX83 fluorescence microscope.

3. Results and discussion

3.1. Backbone cationized HPAEs: Synthesis strategy and transfection performance evaluation

As mentioned in the Introduction, the improved performance of HPAE is attributed to the introduction of more cationic terminal groups compared to LPAE, which play a crucial role in processes like DNA compression, cell recognition, cellular uptake, and endosomal escape. [23–25] Therefore, we hypothesize that introducing additional cationic moieties, building upon an optimized HPAE structure, will enhance the HPAE performance during the intricate transfection process. To introduce cationic moieties in HPAE, the most straightforward strategy would be to increase the branching degree of HPAE thus augmenting the number of cationic terminals. Unfortunately, previous studies have shown that HPAE exhibited optimal gene delivery capabilities at a specific range of branching degrees, beyond which, the HPAE delivery efficiency rapidly declined as the branching degree increased. [24,34] With the above insights, without altering the polymer's topological structure and branching degree, here, we propose a novel structural optimization strategy – incorporating the cationic moieties into the HPAE polymer backbone – to enhance the gene delivery efficiency of HPAE (Fig. 1).

The well-proven efficient HPAE monomer set – BDA, PTTA and S5 as backbone monomers, E7 as the end-capping group – was employed as the structural foundation (Fig. 2A). [35] Based on that, five tertiary amine groups (A-E in Fig. 2A) that are favorable for interaction with DNA were selected to synthesize five types of backbone cationized HPAEs (named as HP1-A to HP1-E, respectively). As a control, the HAPE (i.e., HP1-F) that does not possess additional cationic moieties was also synthesized (Fig. 2A). The GPC results indicated that HP1-A to —F have similar molecular weights and polydispersity as well as branching degrees [$M_{w,GPC}$ = 10 to 14 kDa, $Đ$ = 1.7–2.2, branch degree (BD, molar ratio of PTTA to BDA) = 0.05, Fig. 2B and **Table S4**]. According to the Mark−Houwink (MH) plot (Fig. 2C), an α value between 0.5 and 1.0 signifies a linear structure, while a value below 0.5 suggests a highly branched architecture. [22] It can be seen that HP1-A to —F exhibited close α values ranging from 0.28 to 0.32, demonstrating their similarly highly branched topological structures. The chemical compositions of HP1-A to —F were further confirmed by ^{1}H NMR spectra (Fig. 2D). The appearance of characteristic group signal peaks of A-F provided evidence for the successful introduction of different amine moieties on the HPAE backbones. Moreover, consistent with the feeding ratio (**Table S1**), HP1-A to —F all achieved approximately 20% backbone functionalization ratio (molar ratio of additional amine/(BDA + additional amine)).

After confirming the polymer structures, the transfection capabilities of these HPAEs with different introduced tertiary amines were evaluated by delivering a commercially available plasmid, gWiz, encoding green fluorescent protein, into the disease model—lung CF epithelial (CFBE41o-) cells. In vitro experimental results demonstrated that in

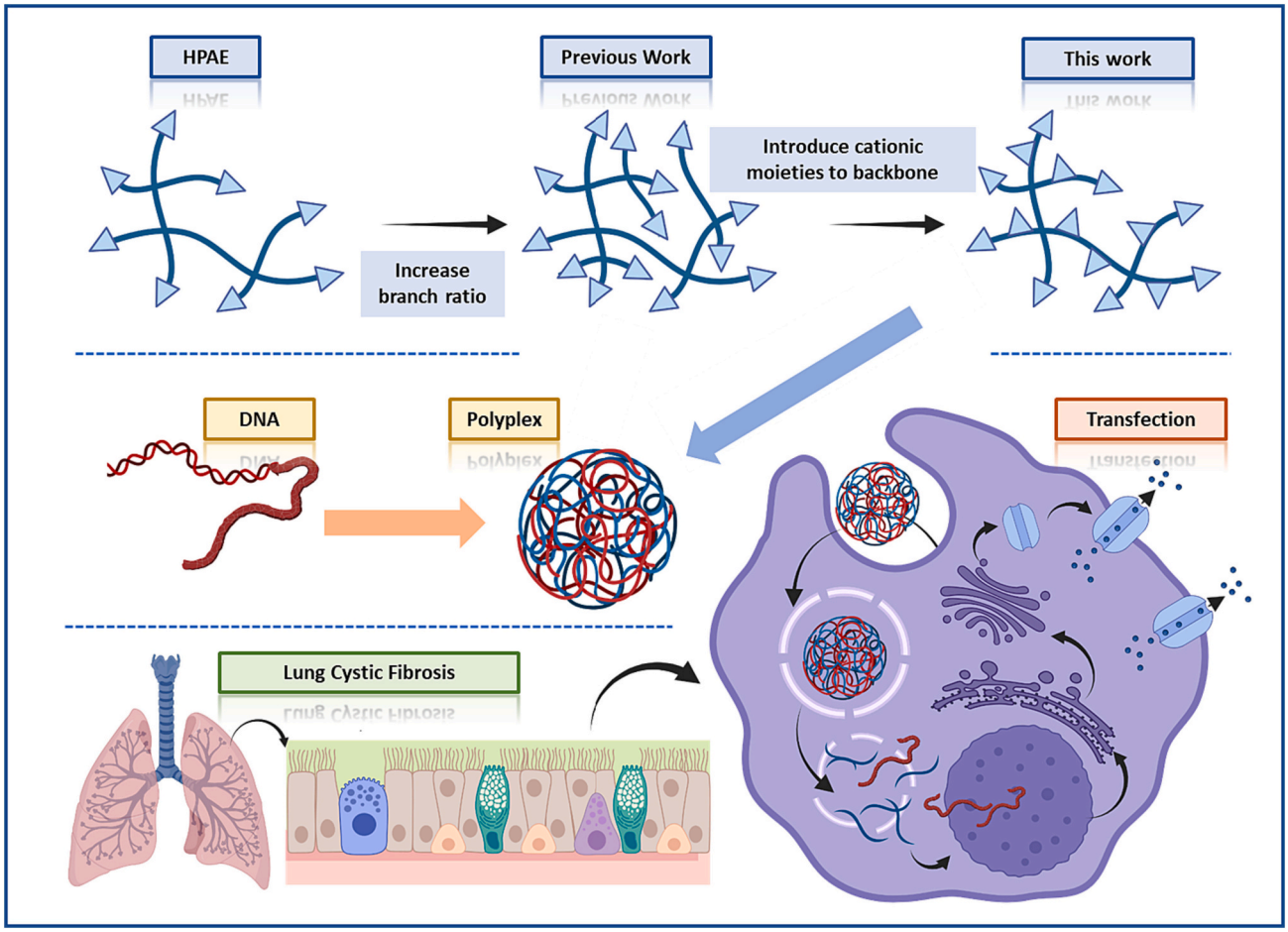

Fig. 1. Schematic illustration of the concept of developing backbone cationized HPAE polyplex system to mediate CFTR protein expression in lung CF epithelial cells.

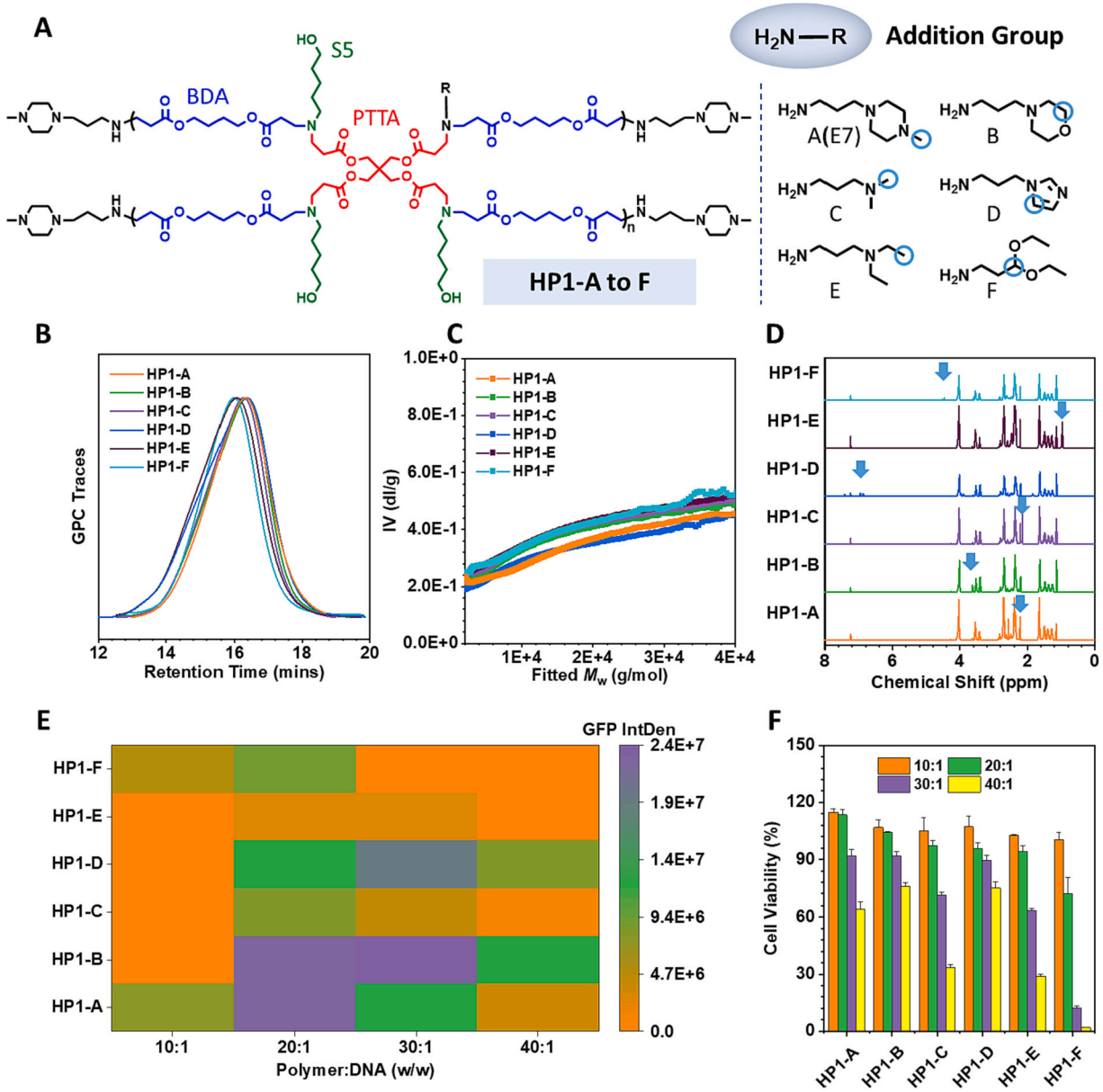

Fig. 2. Structure characterization and transfection performance evaluation of backbone cationized HPAEs with different pendant amine groups. (A) Polymer and monomer chemical structures of HP1-A to —F. Additional tertiary amines structure: A(E7), 1-(3-aminopropyl)-4-methylpiperazine; B(MPA), 3-Morpholinopropylamine; C, 3-(Dimethylamino)-1-propylamine; D, 1-(3-Aminopropyl)imidazole; E, 3-(Diethylamino)propylamine; F, 4-Aminobutyraldehyde diethyl acetal. (B) GPC traces of HP1-A to —F. (C) Mark-Houwink plots of HP1-A to —F. (D) ^{1}H NMR spectra of HP1-A to —F. Blue arrows show the typical peaks for terminal amines corresponding to the proton circled in Fig. 2A. (E) GFP expression of CFBE41o- cells post 48 h transfection by HP1-A to -F-based polyplexes at different polymer/DNA weight ratios (*w*/w). (F) Cell viabilities of CFBE41o- cells post 48 h transfection by HP1-A to -F-based polyplexes at different polymer/DNA ratios. (For interpretation of the references to colour in this figure legend, the reader is referred to the web version of this article.)

general, the backbone cationized HPAEs (HP1-A to -E) all exhibited lower cytotoxicity than that of HP1-F (Fig. 2F). Moreover, the backbone cationized HP1-A and HP1-B exhibited excellent gene delivery capabilities, surpassing those of HP1-C to —F (Fig. 2E). Though the cell viability decreased when the polymer/DNA weight ratio was higher than 30:1, all tested groups maintained nearly 100% cell viability at the best-performed stage with a polymer/DNA weight ratio of 20:1 (Fig. 2F). Notably, the tertiary amines E7 (A in Fig. 2A) and MPA (B in Fig. 2A) introduced in HP1-A and HP1-B are commonly used end-capping groups in the design of highly efficient HPAEs. This suggests that the function mechanism of introduced tertiary amines on transfection is similar to that of HPAE terminal groups, indicating a resemblance in the selection principle of optimal backbone cationization groups and the HPAE end-capping groups in the future.

3.2. Backbone cationized HPAE: Proportion and distribution optimization of cationic moieties towards enhanced transfection performance

Considering the experimental results discussed above, HP1-A (i.e., classical HPAE with the additional introduction of E7 cationic groups into the backbone) demonstrated superior biocompatibility and GFP expression of CFBE41o- cells compared to other HPAE variants (HP1-B to HP1-F) under optimal transfection conditions (polymer/DNA w/w = 20:1), in the following study, further optimization will be focused on the structure of HP1-A.

Proportion optimization of backbone amine groups. The current backbone monomer set for efficient HPAE vectors is the result of screening through thousands of monomer combinations. Therefore, the introduction of different proportions of additional tertiary amines to the

HPAE backbone would affect the transfection efficiency of HPAE vectors at different levels. Based on the preliminary screening results from the above section, to further enhance the backbone cationized HPAE gene delivery efficiency, an optimal proportion of the extra introduced E7 cationic groups needs to be found. To address this, HP2-A to —F with a series of backbone E7 molar ratios (HP2-A - 0%, HP2-B - 5%, HP2-C - 10%, HP2-D - 20%, HP2-E - 30%, HP2-F - 50%, calculated according to the molar ratio of S5/all amine groups on polymer backbone) were prepared (**Table S2,** Fig. 3A). Among these, HP2-A represents a typical HPAE without the additional introduction of cationic amine groups, and HP2-D is the same as the previously mentioned HP1-A (**Table S1,** Fig. 2B). The structures of these HPAE variants were also confirmed by GPC and ^{1}H NMR. GPC traces demonstrate that these HPAEs have similar molecular weights, *Đ* and BDs (Fig. 3B**,** Fig. 3D**, Table S5**). Additionally, their Mark-Houwink indexes all fall between 0.29 and 0.32, suggesting similar branching topologies (Fig. 3C). ^{1}H NMR spectra confirmed the increase of the E7 ratio (from 0% to 50%) from HP2-A to —F (Fig. 3D).

Subsequently, HP2-A to HP2-F were applied to transfection studies in CFBE41o- cells. As shown in Fig. 3E, as the ratio of introduced E7 cationic amines increases, the gene delivery efficiency of HPAE initially increases and then decreases. The optimal transfection efficiency was achieved by HP2-C (with 10% E7 group), which significantly surpassed HP2-A (without additional pendant amines) and outperformed HP2-D (i.e., HP1-A in the former section). In terms of cell viability, the performances of HP2-A to -E are similar, though with the increase in additional cationic moieties, cell toxicity also slightly increased (Fig. 3F). Particularly, at a high polymer/DNA *w*/w ratio of 40:1, cells transfected with HP2-F exhibited only ca. 30% cell viability (Fig. 3F), which may be attributed to the disrupted cell membrane structure by an excess of cationic groups, causing cytotoxicity.

Distribution optimization of backbone amine groups. The above

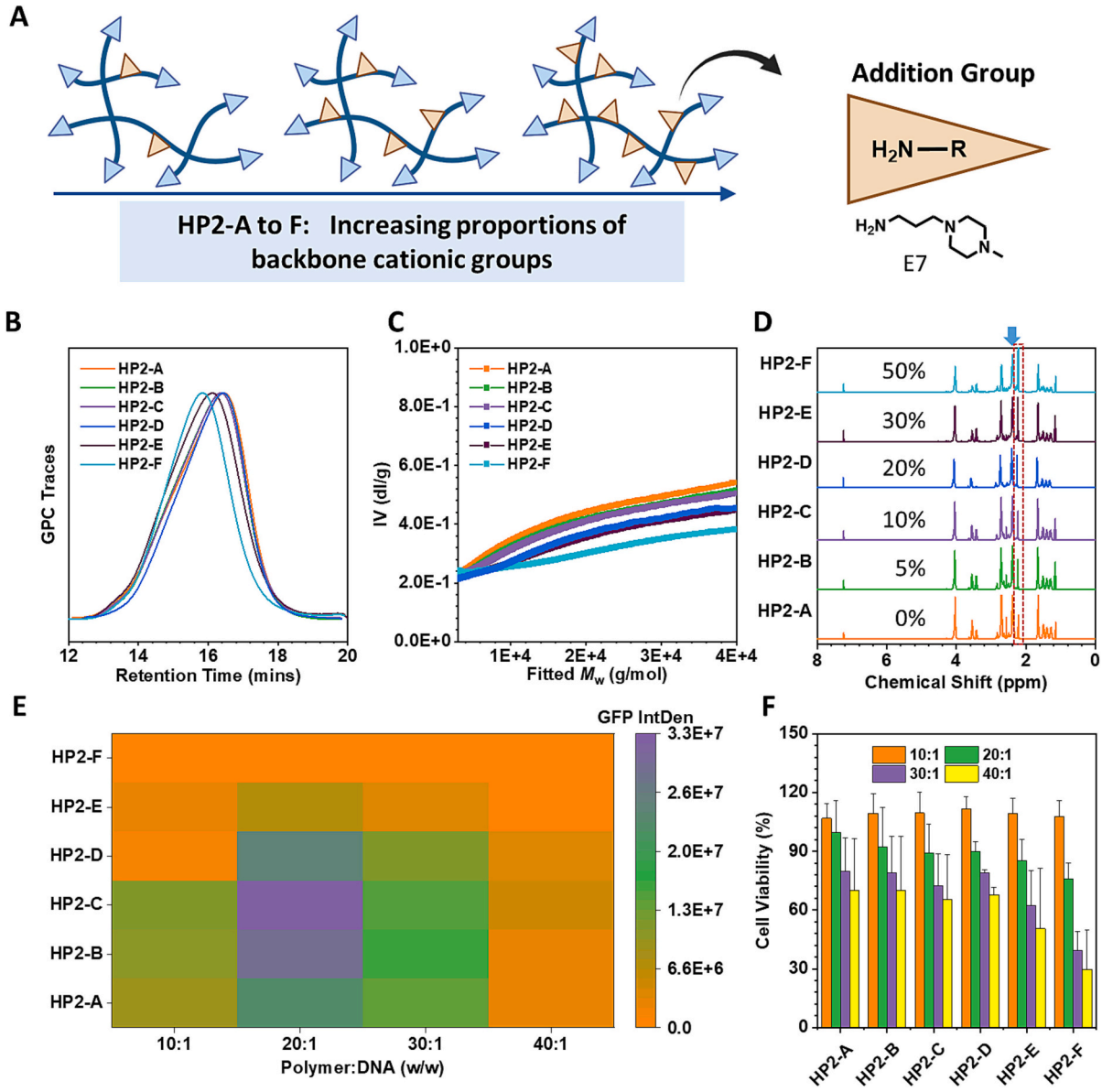

Fig. 3. Structure characterization and transfection performance evaluation of backbone cationized HPAEs with different proportions of E7 amine groups. (A) Schematic illustration of the HPAE polymer structural changes from HP2-A to —F. (B) GPC traces of HP2-A to —F. (C) Mark-Houwink plots of HP2-A to —F. (D) ^{1}H NMR spectra of HP2-A to —F. The percentage of E7 was calculated as the molar ratio of E7/(E7 + S5) on polymer backbone. The bule arrow shows the increased amount of E7 groups from HP2-A to —F. (E) GFP expression of CFBE41o- cells post 48 h transfection by HP2-A to -F-based polyplexes at different polymer/DNA ratios. (F) Cell viabilities of CFBE41o- cells post 48 h transfection by HP2-A to -F-based polyplexes at different polymer/DNA weight ratios.

results demonstrate that introducing a certain proportion (approximately 10%) of cationic tertiary amines in the HPAE backbone significantly enhanced their gene delivery efficiency. However, unlike the end-capping cationic amino groups (which are located at the flexible chain ends and are favorable for contact with DNA or other molecules), the E7 amino groups introduced into the HPAE backbone are randomly distributed within the molecular framework. Many of these cationic groups may be buried within the molecular structure, hindering their interaction with DNA or other molecules, and limiting their transfection effectiveness. To address this, we further attempted to modulate the distribution of backbone cationic groups within the HPAE molecule and explore the impact of this distribution on transfection behavior (Fig. 4).

As depicted in Fig. 4, HP3-A to HP3-E were synthesized with 10% E7 cationic moieties incorporated in the backbone but distributed in different modes (**Table S3**). HP3-A is the HP2-C that was discussed in the above section, it was synthesized through a one-step direct Michael addition approach, where the E7 cationic groups were randomly dispersed within the HPAE molecular backbone framework. HP3-B was prepared using a three-step method. First, the monomers BDA, PTTA, and S5 were polymerized to form the basic backbone (Step 1). Then, the cationic monomer E7 was polymerized with additional BDA to form a batch of short chains (Step 2). In Step 3, the polymer precursor synthesized from Step 1 and the polymer precursor synthesized from Step 2 were then combined via Michael addition, thus HP3-B was obtained with the additional E7 cationic groups located on the exterior of the HPAE molecular backbone (**Fig. S12** to **S14, Fig. S22**). For the synthesis of HP3-C, a long chain of E7/BDA was first prepared (Step 1), which was then mixed and reacted with other backbone monomers (BDA, PTTA, and S5) (Step 2). HP3-C was then yielded, containing a dense long chain of pendant tertiary amines (**Fig. S15** and **S16, Fig. S23**). HP3-D features a structure with E7 amine groups located within the molecular interior (**Fig. S17** to **S19, Fig. S24**). Initially, PTTA and E7 were polymerized to prepare a branched core (Step 1). Subsequently, a short-chain backbone was synthesized by BDA and S5 (Step 2). Finally, the two segments were connected to enable cationic E7 tertiary amines to be positioned within the interior of the HP3-D backbone (Step 3). Lastly, the block copolymer HP3-E was prepared using a two-step method. First, a short chain consisting of E7/BDA was obtained (Step 1). Then, the short chains were copolymerized with other backbone monomers (BDA, PTTA, and S5) to yield the final product – HP3-E (**Fig. S20** and **S21, Fig. S25**), in which the E7 groups were randomly distributed in blocks on the HPAE backbone. The chemical structures of HP3-A to -E (similar $M_{w,GPC}$, $Đ$, BDs, and E7 proportions on backbone) were confirmed by ^{1}H NMR and GPC (Fig. 4**, Fig. S22** to **S25**).

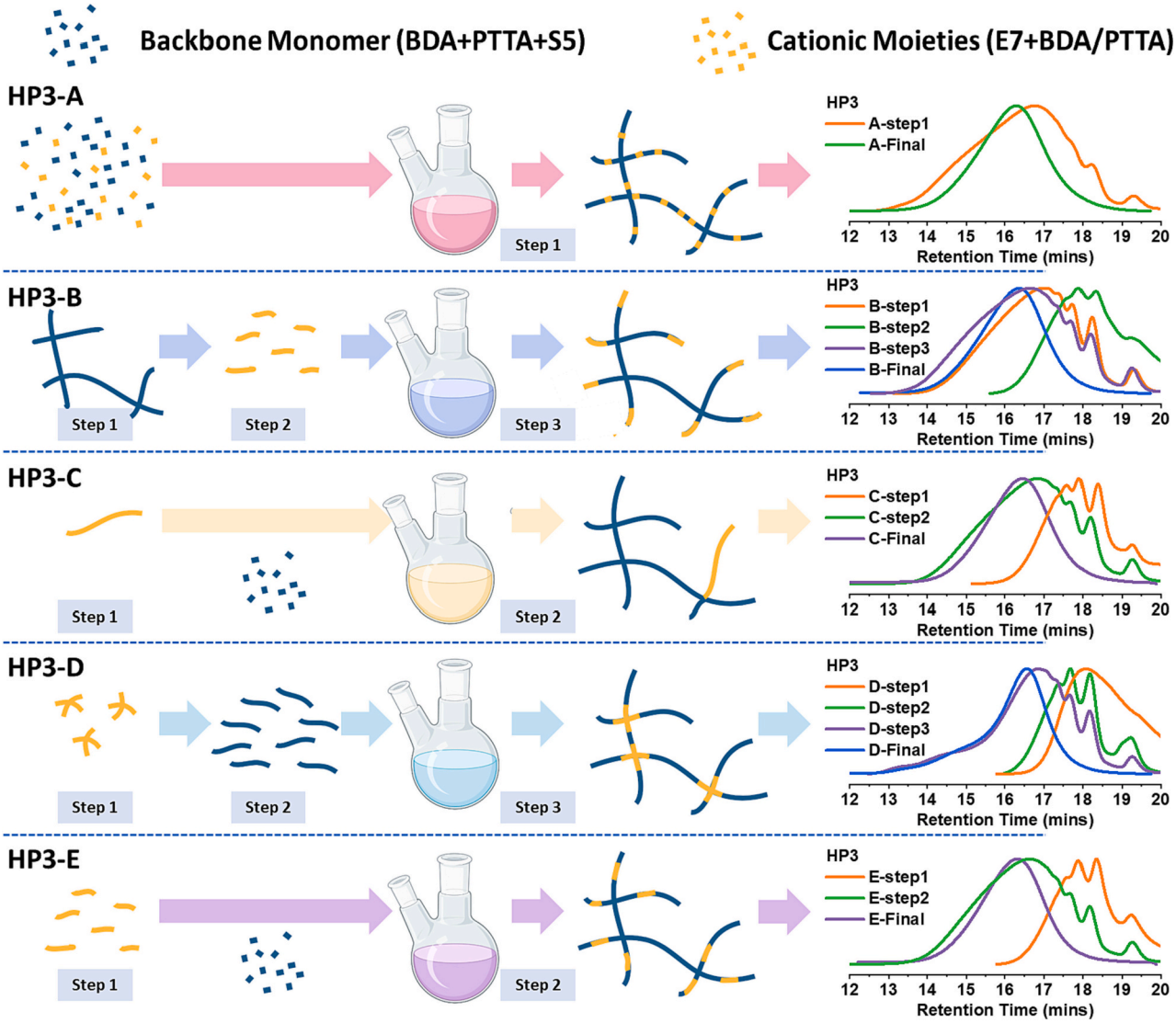

Fig. 4. Schematic illustration of the different synthesis strategies towards HP3-A to -E with different backbone cationic amine group distributions, as well as their GPC traces.

To comprehensively assess the gene delivery capabilities of HP3-A to -E, three typical cell lines related to lung CF disease were selected as in vitro evaluation models. HBE represents primary human normal lung epithelial cells, CFBE41o- cells represent epithelial cells with lung CF pathology, and A549 cells represent transformed lung epithelial cells. In vitro transfection results revealed that, after 48 h of transfection, HP3-E, featuring a backbone cationized HPAE polymer with random block tertiary amine distribution, exhibited the most efficient gene delivery in CFBE41o- disease cells (Fig. 5A) and the highest cell viability (Fig. 5B). Additionally, in CFBE41o- disease cells, the optimal polymer/DNA *w*/w ratio for all HPAEs (HP3-A to -E) was 20:1, with transfection efficiency declining to varying degrees beyond this ratio (Fig. 5A). Apart from the high HPAE dose group (polymer/DNA w/w = 40:1), all transfection groups showed low biological toxicity, maintaining >90% cell viability (Fig. 5B). Unexpectedly, in the cancer cell line A549, HP3-A and HP3-C demonstrated superior transfection efficiency. The optimal polymer/DNA w/w ratio was still 20:1, while post-transfection, cell viability showed a noticeable decrease compared to that in CFBE41o-, with cells maintaining 75%–90% viability (**Fig. 5C** and **D**). Regarding the primary HBE transfection, HP3-A, with randomly distributed cationic backbone

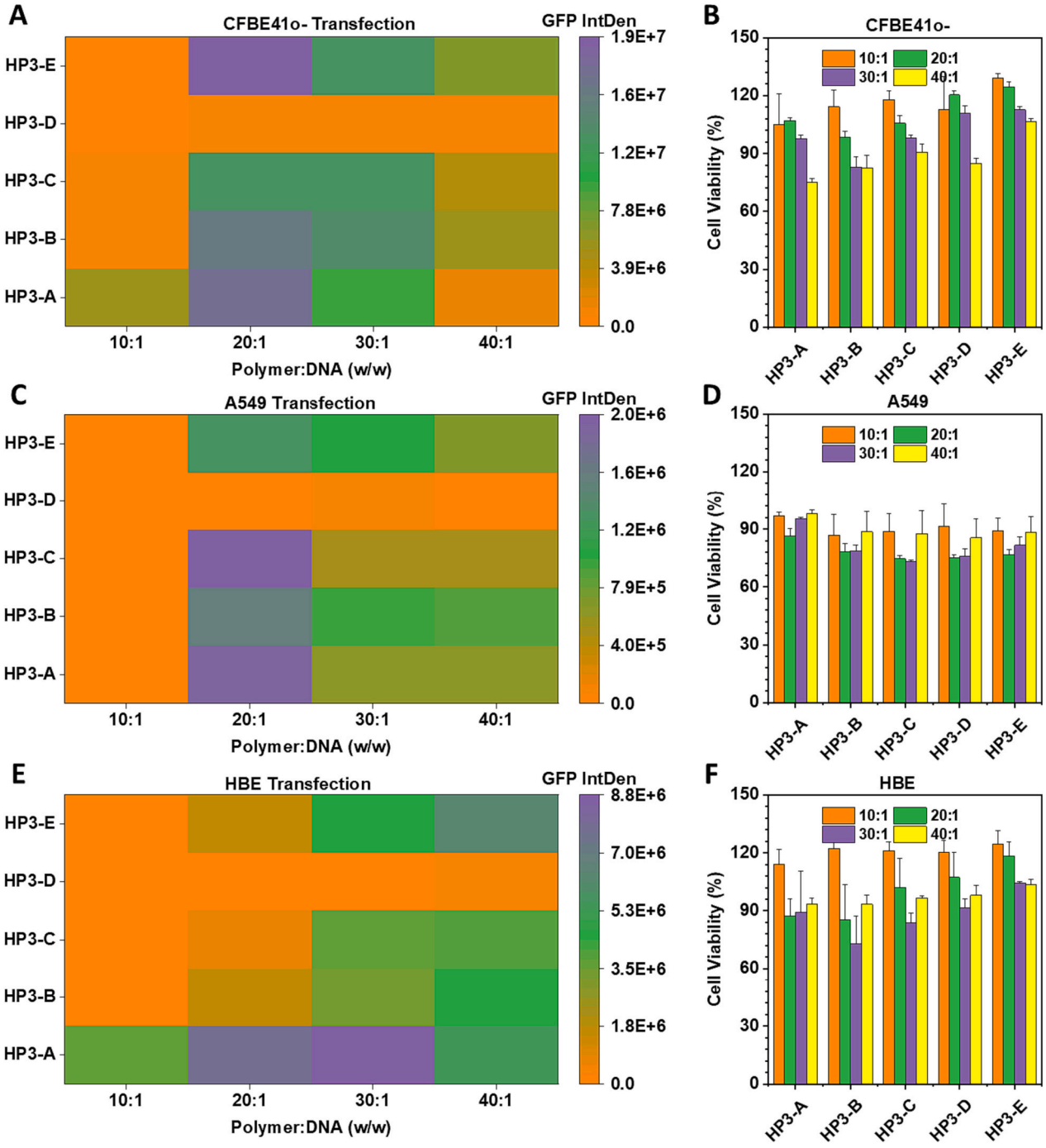

Fig. 5. In vitro evaluation of transfection performance of HPAE with different cationic amine group distributions in three types of cell lines. (A) GFP expression and (B) Cell viabilities of CFBE41o- cells post 48 h transfection by HP3-A to -E-based polyplexes at different polymer/DNA weight ratios. (C) GFP expression and (D) Cell viabilities of A549 cells post 48 h transfection by HP3-A to -E-based polyplexes at different polymer/DNA weight ratios. (E) GFP expression and (F) Cell viabilities of HBE cells post 48 h transfection by HP3-A to -E-based polyplexes at different polymer/DNA weight ratios.

groups, achieved the best transfection efficiency at a polymer/DNA w/w ratio of 30:1. Unlike the behaviors in other two cell types, the gene delivery efficiency of HP3-B to HP3-E increased with the rise in polymer/DNA weight ratios (Fig. 5**E** and **F**). It is noteworthy that HP3-D, with cationic amine groups distributed near the branching cores, showed the lowest transfection efficiency in all three cell types. This aligns with our expectation above, that is, the additional cationic amines located within the interior of the backbone would be buried within the molecular structure, hindering their interaction with DNA or other molecules, thus ineffective in enhancing transfection efficiency.

Considering the differences between cells, the transfection behaviors of HPAEs in CFBE41o- cells, HBE and A549 might be different, the research will focus on transfection target disease cells (CFBE41o- cells) in the following research. Therefore, to further explore the differences in transfection behavior among HPAEs with different cationic amine distribution, the transfection behaviors of HP3-A to -E were further examined in terms of several key steps during the transfection process in the disease model. Successful DNA condensation and packaging, which protect DNA from endonuclease degradation and facilitate polyplex cellular uptake, are prerequisites for successful gene transfection.

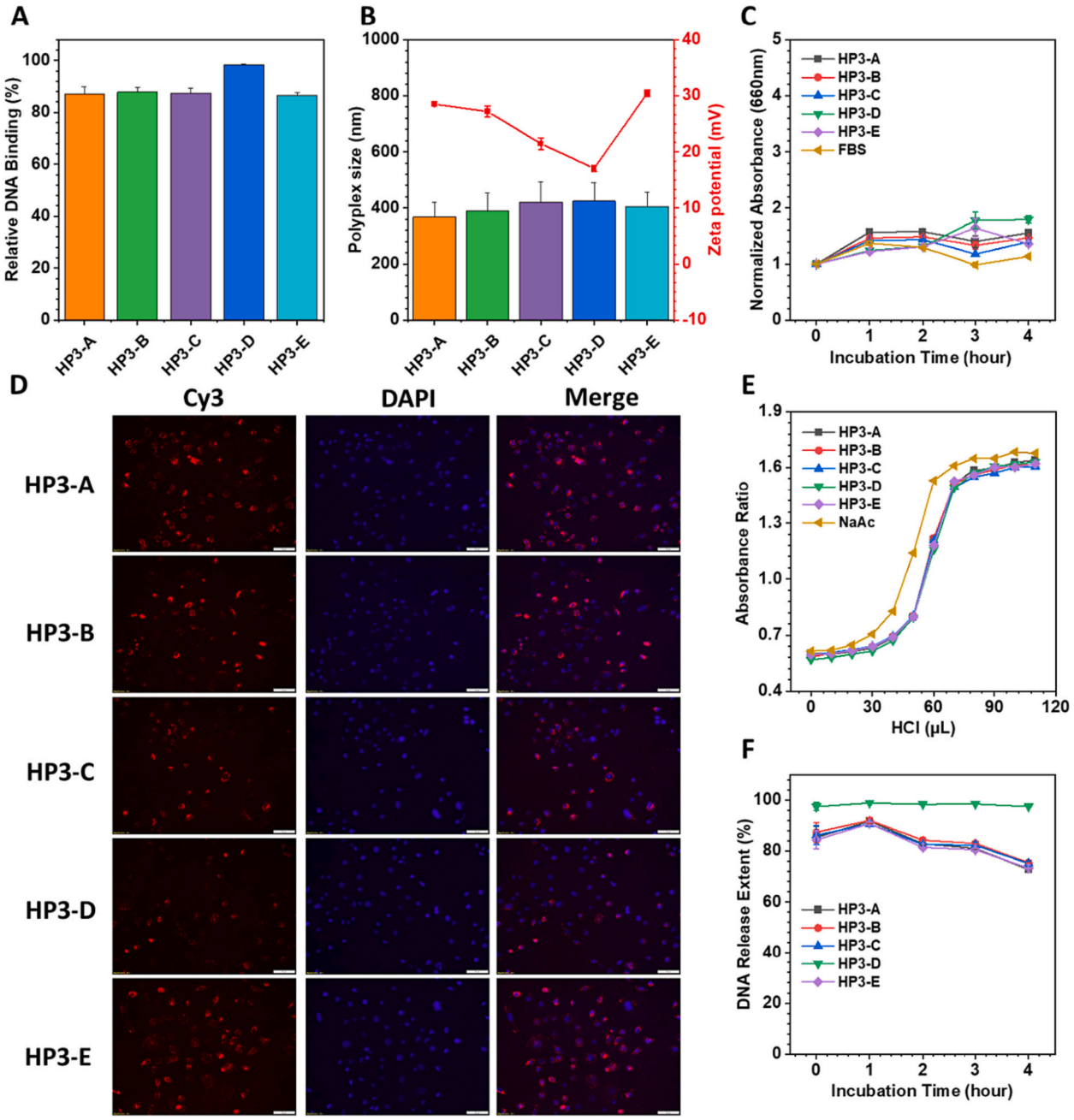

Fig. 6. In vitro investigation of the gene transfection performance of HP3-A to -E during the key steps in gene transfection process. (A) Assessment of the DNA binding capability of HP3-A to -E at polymer/DNA weight ratio (*w*/w) of 20:1 using the PicoGreen assay. (B) Particle size and zeta potential of HP3-A to -E -based polyplexes. (C) Serum stability of HP3-A to -E polyplexes at polymer/DNA weight ratio (w/w) of 20:1, assessed by the UV absorbance at 660 nm with 10% FBS at 37 °C. The polyplexes size evaluation at 0 and 4 h was repeated in triplicate. (D) Cellular uptake of HP3-A to -E polyplexes, evaluated by the fluorescence of the Cy3-labeled DNA of CFBE41o- cells 4 h post-transfection. (E) Proton buffer capability of HP3-A to -E-based polyplexes evaluated by the ratio of UV absorbance at 508 nm and 468 nm with 0.01% methyl orange. 25 mM Sodium Acetate buffer (NaAc) was served as control. (F) DNA protection capability of HP3-A to -E under acidic conditions (25 mM sodium acetate), evaluated by DNA binding efficiency at 37 °C using a PicoGreen assay.

Therefore, the DNA binding efficiency of HP3-A to -E was initially studied by PicoGreen Assay. The results showed that all HPAEs exhibited high binding efficiency (>80%) across a range of polymer/DNA weight ratios, surpassing 85% at the optimal polymer/DNA ratio of 20:1 (Fig. 6A, **Fig. S27**). All HPAEs successfully bound to DNA, forming polyplexes with a size of approximately 400 nm (Fig. 6B). DLS testing results showed that HP3-A and HP3-E exhibited a high positive potential of around 30 mV, which is favorable for cellular uptake (Fig. 6B). In contrast, HP3-C and HP3-D had a relatively low surface potential (approximately 20 mV), indicating that the pendant cationic long chain of tertiary amines within the backbone and the concentrated distribution of amine groups within the interior of the backbone were not easily exposed on the outer surface of the nanoparticles, hindering interaction with cells.

Before achieving effective cellular uptake, polyplexes need to remain stable in physiological conditions. Previous studies have demonstrated that nanoparticles with a positive surface charge are prone to binding with proteins in the physiological environment, leading to aggregation and eventual clearance by the immune system, rendering them ineffective. [36,37] Therefore, the serum stability of nanoparticles based on HP3-A to -E was further characterized.

The results showed that all polyplexes remained stable at polymer/DNA w/w ratios ranging from 10:1 to 40:1 under 10% serum conditions within four hours (Fig. 6C, **Fig. S28** to **S30**). Subsequently, cellular uptake of different polyplexes was evaluated using CFBE41o- cells in the CF disease model, with transfection marked by Cy3-labeled DNA. According to fluorescence images (Fig. 6D), the trend of cellular uptake aligned with the variation in transfection efficiency among different HPAEs. Compared to other HPAEs, HP3-A and HP3-E with randomly distributed backbone cationic groups demonstrated higher cellular uptake. Furthermore, this observation was consistent with the high surface potential results of HP3-A and HP3-E obtained from DLS testing. Furthermore, once polyplexes are successfully internalized by cells, they need to overcome the barriers of endosomal escape, protect DNA from acidic degradation, and ultimately release DNA in the cytoplasm. Therefore, the proton buffer and DNA protection capabilities of HP3-A to -E polyplexes were assessed. The results showed that under all conditions, all HPAEs exhibited good proton buffer (Fig. 6E, **Fig. S31** to **S33**) and DNA protection capabilities (Fig. 6F, **Fig. S34** to **S36**). Overall, the above analysis indicates that the distribution of cationic groups in the polymer backbone impacted the transfection results by affecting the surface positive charge of polyplexes and influencing cellular uptake in the CFBE41o- disease model.

3.3. *Backbone cationized HPAE-mediated gene therapy in lung CF disease models*

While the HPAE delivery vector has demonstrated high-level reporter gene expression in the commercialized plasmid gWiz delivery, achieving successful translation in delivering large functional gene constructs poses a more formidable challenge. According to the above comparison, the top-performed HPAE vectors in CFBE41o- cells (target

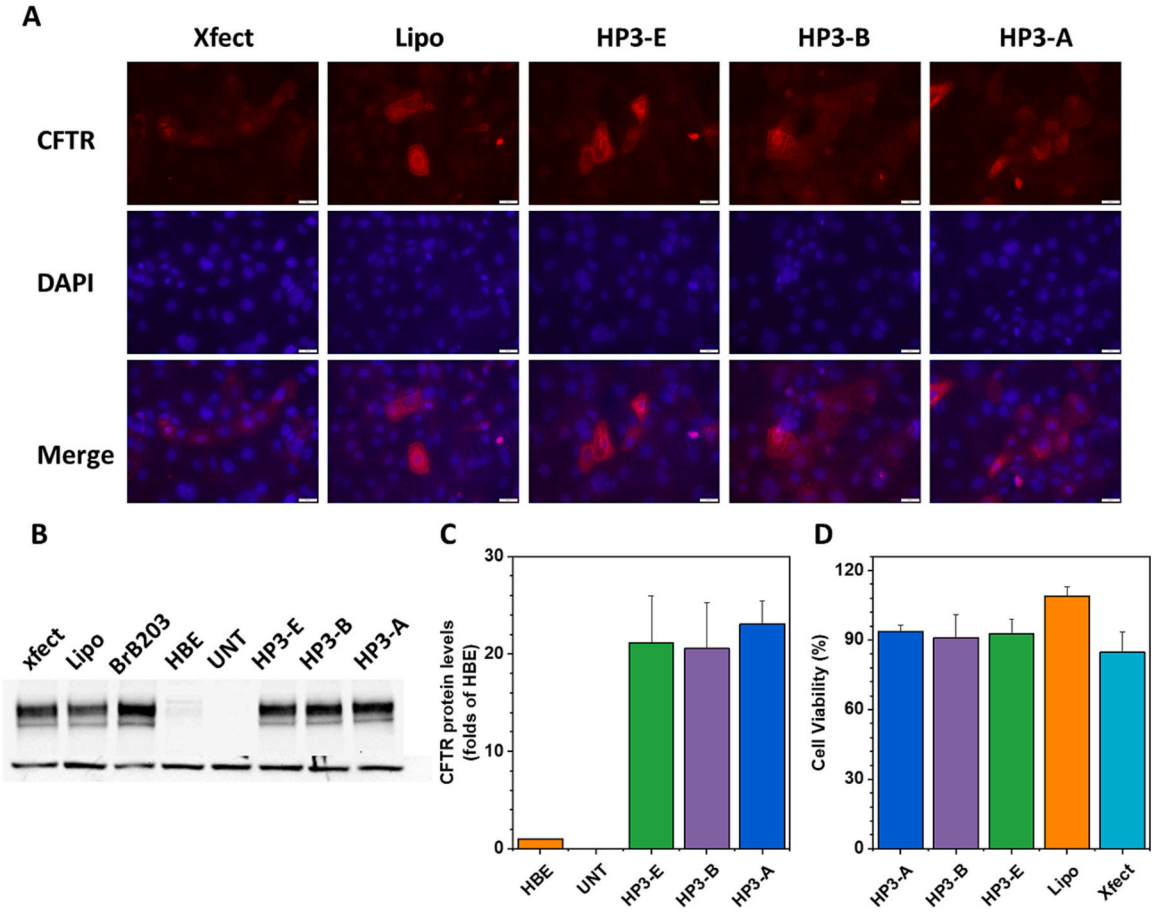

Fig. 7. CFTR expression and function restoration of backbone cationized HPAE/CpG-deplete CFTR plasmid polyplexes in CFBE41o- cells. (A) Immunocytochemistry images of CFBE41o- cells after 48 h transfection with backbone cationized HPAE/CpG-deplete CFTR plasmid complexes. Commercial reagents - Lipofectamine3000, Xfect and BrB203 were used as controls. CFTR was detected in red, and the nucleus was stained by DAPI in blue, using a 40× fluorescence microscopy objective. (B) CFTR protein expression by western blot. (C) Semi-quantified CFTR protein expression by western blot normalized by α-Tubulin. (D) Cell viabilities of CFBE41o- cells post 48 h transfection by CpG-deplete CFTR plasmid polyplexes. (For interpretation of the references to colour in this figure legend, the reader is referred to the web version of this article.)

for lung cystic fibrosis gene therapy), HP3-A, HP3-B, and HP3-E, were selected to be loaded with a therapeutic plasmid, CpG-deplete CFTR plasmid, [38] aiming to manipulate CFTR protein for the construction of a gene therapy system for pulmonary CF.

The therapeutic efficacy of this system was validated by assessing the restoration of CFTR protein expression in the CFBE41o- disease model. Fig. 7A outlines the cell immunofluorescence images of CFBE41o- cells two days after transfection with backbone cationized HPAE/CpG-deplete CFTR plasmid polyplex. The group treated with the state-of-the-art commercial reagents Xfect and Lipofectamine 3000 showed moderate fluorescence, indicating CFTR production. In contrast, CFBE41o- cells transfected with backbone cationized HPAE/CpG-deplete CFTR plasmid polyplexes displayed the strong fluorescence, suggesting enhanced CFTR expression obtained through backboned cationized HPAEs. Further quantitative assessment of CFTR expression efficiency was conducted through Western blotting studies (Fig. 7B). Consistent with the previous report, all three groups transfected with backbone cationized HPAE/CpG-deplete CFTR plasmid polyplexes exhibited a significant enhancement in CFTR expression compared to the commercial reagents group, reaching 20–23 times that of normal HBE cells (Fig. 7C), while maintain >90% cell viability Fig. 7D.

4. Conclusion

In summary, building upon the classical gene delivery vector HPAE, a backbone cationization optimization strategy was proposed to synthesize a series of more efficient HPAE gene delivery vectors by introducing additional cationic amine groups to the polymer backbone without altering the branching degree. Through the modulation of the type, proportion, and intra-molecular backbone distribution of the introduced cationic amine groups, highly efficient gene delivery vectors for treating CF disease were successfully constructed. HP3-A, B, and E, when loaded with therapeutic plasmids, successfully restored CFTR protein expression in the CFBE41o- disease model, achieving levels 20–23 times that of normal HBE cells. Their therapeutic efficacy also far surpassed that of the currently most advanced commercial vectors, Xfect and Lipofectamine 3000. The innovative backbone cationization strategy will significantly contribute to the future design and development of high-performance non-viral polymeric gene carriers for gene therapy applications.

CRediT authorship contribution statement

Yinghao Li: Writing – original draft, Methodology, Investigation, Funding acquisition, Formal analysis, Conceptualization. **Bei Qiu:** Writing – original draft, Methodology, Investigation, Formal analysis. **Zishan Li:** Investigation, Data curation. **Xianqing Wang:** Data curation. **Zhonglei He:** Data curation. **Darío Manzanares Sandoval:** Methodology. **Rijian Song:** Formal analysis, Data curation. **A. Sigen:** Data curation. **Chunyu Zhao:** Formal analysis. **Melissa Johnson:** Writing – review & editing. **Jing Lyu:** Writing – review & editing, Supervision, Project administration, Funding acquisition, Conceptualization. **Irene Lara-Sáez:** Data curation. **Wenxin Wang:** Writing – review & editing, Supervision, Conceptualization.

Declaration of competing interest

The authors declare no competing financial interest.

Data availability

Data will be made available on request.

Acknowledgements

This research was supported by the Chinese Government—China Scholarship Council (CSC202008300033), Science Foundation Ireland (SFI) Frontiers for the Future 2019 call (19/FFP/6522), and the Irish Research Council (IRC) Government of Ireland Postdoctoral Fellowship (GOIPD/2022/209).

Appendix B. Supplementary data

Supplementary figures show ^{1}H NMR spectra and GPC traces of all HPAEs. Serum stabilities, proton buffer capabilities, DNA binding efficiencies, DNA protection capabilities of HPAE-based polyplexes at different polymer/DNA weight ratios. Supplementary tables show monomer feed ratios for different HPAEs synthesis, and ^{1}H NMR and GPC characterization results for different HPAEs. Supplementary data to this article can be found online at https://doi.org/10.1016/j.jconrel.2024.01.046.

References

[1] M. Shteinberg, I.J. Haq, D. Polineni, J.C. Davies, Cystic fibrosis, Lancet (London, England). 397 (2021) 2195–2211, https://doi.org/10.1016/S0140-6736(20)32542-3.
[2] J.R. Riordan, J.M. Rommens, B.-S. Kerem, N. Alon, R. Rozmahel, Z. Grzelczak, J. Zielenski, S. Lok, N. Plavsic, J.-L. Chou, M.L. Drumm, M.C. Iannuzzi, F.S. Collins, L.-C. Tsui, Identification of the cystic fibrosis gene: cloning and characterization of complementary DNA, Science (80-.) 245 (1989) 1066–1073, https://doi.org/10.1126/science.2475911.
[3] A.A. Pezzulo, X.X. Tang, M.J. Hoegger, M.H. Abou Alaiwa, S. Ramachandran, T. O. Moninger, P.H. Karp, C.L. Wohlford-Lenane, H.P. Haagsman, M. van Eijk, B. Bánfi, A.R. Horswill, D.A. Stoltz, P.B. McCray, M.J. Welsh, J. Zabner, Reduced airway surface pH impairs bacterial killing in the porcine cystic fibrosis lung, Nature. 487 (2012) 109–113, https://doi.org/10.1038/nature11130.
[4] C. Castellani, A.J.A. Duff, S.C. Bell, H.G.M. Heijerman, A. Munck, F. Ratjen, I. Sermet-Gaudelus, K.W. Southern, J. Barben, P.A. Flume, P. Hodková, N. Kashirskaya, M.N. Kirszenbaum, S. Madge, H. Oxley, B. Plant, S. J. Schwarzenberg, A.R. Smyth, G. Taccetti, T.O.F. Wagner, S.P. Wolfe, P. Drevinek, ECFS best practice guidelines: the 2018 revision, J. Cyst. Fibros. 17 (2018) 153–178, https://doi.org/10.1016/j.jcf.2018.02.006.
[5] S.M. Rowe, C. Daines, F.C. Ringshausen, E. Kerem, J. Wilson, E. Tullis, N. Nair, C. Simard, L. Han, E.P. Ingenito, C. McKee, J. Lekstrom-Himes, J.C. Davies, Tezacaftor–ivacaftor in residual-function heterozygotes with cystic fibrosis, N. Engl. J. Med. 377 (2017) 2024–2035, https://doi.org/10.1056/NEJMoa1709847.
[6] G.J. Connett, Lumacaftor-ivacaftor in the treatment of cystic fibrosis: design, development and place in therapy, Drug Des. Devel. Ther. 13 (2019) 2405–2412, https://doi.org/10.2147/DDDT.S153719.
[7] K. Ridley, M. Condren, Elexacaftor-tezacaftor-ivacaftor: the first triple-combination cystic fibrosis transmembrane conductance regulator modulating therapy, J. Pediatr. Pharmacol. Ther. 25 (2020) 192–197, https://doi.org/10.5863/1551-6776-25.3.192.
[8] U. Griesenbach, K.M. Pytel, E.W.F.W. Alton, Cystic fibrosis gene therapy in the UK and elsewhere, Hum. Gene Ther. 26 (2015) 266–275, https://doi.org/10.1089/hum.2015.027.
[9] A.L. Cooney, P.B. McCray, P.L. Sinn, Cystic fibrosis gene therapy: looking back, looking forward, Genes (Basel) 9 (2018), https://doi.org/10.3390/genes9110538.
[10] J.B. Zuckerman, C.B. Robinson, K.S. McCoy, R. Shell, T.J. Sferra, N. Chirmule, S. A. Magosin, K.J. Propert, E.C. Brown-Parr, J.V. Hughes, J. Tazelaar, C. Baker, M. J. Goldman, J.M. Wilson, A phase I study of adenovirus-mediated transfer of the human cystic fibrosis transmembrane conductance regulator gene to a lung segment of individuals with cystic fibrosis, Hum. Gene Ther. 10 (1999) 2973–2985, https://doi.org/10.1089/10430349950016384.
[11] I. Lostalé-Seijo, J. Montenegro, Synthetic materials at the forefront of gene delivery, Nat. Rev. Chem. 2 (2018) 258–277, https://doi.org/10.1038/s41570-018-0039-1.
[12] A. Shahryari, I. Burtscher, Z. Nazari, H. Lickert, Engineering gene therapy: advances and barriers, Adv. Ther. 4 (2021) 2100040, https://doi.org/10.1002/adtp.202100040.
[13] L. Naldini, Gene therapy returns to Centre stage, Nature. 526 (2015) 351–360, https://doi.org/10.1038/nature15818.
[14] E. Robinson, K.D. MacDonald, K. Slaughter, M. McKinney, S. Patel, C. Sun, G. Sahay, Lipid nanoparticle-delivered chemically modified mRNA restores chloride secretion in cystic fibrosis, Mol. Ther. 26 (2018) 2034–2046, https://doi.org/10.1016/j.ymthe.2018.05.014.
[15] E.W.F.W. Alton, M. Stern, R. Farley, A. Jaffe, S.L. Chadwick, J. Phillips, J. Davies, S.N. Smith, J. Browning, M.G. Davies, M.E. Hodson, S.R. Durham, D. Li, P. K. Jeffery, M. Scallan, R. Balfour, S.J. Eastman, S.H. Cheng, A.E. Smith, D. Meeker, D.M. Geddes, Cationic lipid-mediated CFTR gene transfer to the lungs and nose of patients with cystic fibrosis: a double-blind placebo-controlled trial, Lancet. 353 (1999) 947–954, https://doi.org/10.1016/S0140-6736(98)06532-5.
[16] F.E. Ruiz, J.P. Clancy, M.A. Perricone, Z. Bebok, J.S. Hong, S.H. Cheng, D. P. Meeker, K.R. Young, R.A. Schoumacher, M.R. Weatherly, L. Wing, J.E. Morris, L. Sindel, M. Rosenberg, F.W. van Ginkel, J.R. McGhee, D. Kelly, R.K. Lyrene, E.

J. Sorscher, A clinical inflammatory syndrome attributable to aerosolized lipid–DNA administration in cystic fibrosis, Hum. Gene Ther. 12 (2001) 751–761, https://doi.org/10.1089/104303401750148667.
[17] Y.K. Sung, S.W. Kim, Recent advances in polymeric drug delivery systems, Biomater. Res. 24 (2020) 12, https://doi.org/10.1186/s40824-020-00190-7.
[18] J. Chen, K. Wang, J. Wu, H. Tian, X. Chen, Polycations for gene delivery: dilemmas and solutions, Bioconjug. Chem. 30 (2018) 338–349, https://doi.org/10.1021/acs.bioconjchem.8b00688.
[19] A. Aied, U. Greiser, A. Pandit, W. Wang, Polymer gene delivery: overcoming the obstacles, Drug Discov. Today 18 (2013) 1090–1098, https://doi.org/10.1016/j.drudis.2013.06.014.
[20] S. Iqbal, Y. Qu, Z. Dong, J. Zhao, A. Rauf Khan, S. Rehman, Z. Zhao, Poly (β-amino esters) based potential drug delivery and targeting polymer; an overview and perspectives, Eur. Polym. J. 141 (2020) 110097, https://doi.org/10.1016/j.eurpolymj.2020.110097.
[21] S. Iqbal, Z. Zhao, Poly (β amino esters) copolymers: novel potential vectors for delivery of genes and related therapeutics, Int. J. Pharm. 611 (2022) 121289, https://doi.org/10.1016/j.ijpharm.2021.121289.
[22] M. Zeng, Q. Xu, D. Zhou, A. Sigen, F. Alshehri, I. Lara-Sáez, Y. Zheng, M. Li, W. Wang, Highly branched poly(β-amino ester)s for gene delivery in hereditary skin diseases, Adv. Drug Deliv. Rev. 176 (2021) 113842, https://doi.org/10.1016/j.addr.2021.113842.
[23] Y. Li, X. Wang, Z. He, M. Johnson, A. Sigen, I. Lara-Sáez, J. Lyu, W. Wang, 3D macrocyclic structure boosted gene delivery: multi-cyclic poly(β-amino ester)s from step growth polymerization, J. Am. Chem. Soc. 145 (2023) 17187–17200, https://doi.org/10.1021/jacs.3c04191.
[24] Y. Li, X. Wang, Z. He, Z. Li, M. Johnson, B. Qiu, R. Song, A. Sigen, I. Lara-Sáez, J. Lyu, W. Wang, A new optimization strategy of highly branched poly(β-amino ester) for enhanced gene delivery: removal of small molecular weight components, Polymers (Basel) 15 (2023) 1518, https://doi.org/10.3390/polym15061518.
[25] W. Wang, D. Zhou, L. Cutlar, Y. Gao, W. Wang, J. O'Keeffe-Ahern, S. McMahon, B. Duarte, F. Larcher, B.J. Rodriguez, U. Greiser, The transition from linear to highly branched poly(β-amino ester)s: branching matters for gene delivery, Sci. Adv. 2 (2016) e1600102, https://doi.org/10.1126/sciadv.1600102.
[26] D.M. Lynn, R. Langer, Degradable poly(β-amino esters): synthesis, characterization, and self-assembly with plasmid DNA, J. Am. Chem. Soc. 122 (2000) 10761–10768, https://doi.org/10.1021/ja0015388.
[27] A. Abramson, A.R. Kirtane, Y. Shi, G. Zhong, J.E. Collins, S. Tamang, K. Ishida, A. Hayward, J. Wainer, N.U. Rajesh, X. Lu, Y. Gao, P. Karandikar, C. Tang, A. Lopes, A. Wahane, D. Reker, M.R. Frederiksen, B. Jensen, R. Langer, G. Traverso, Oral mRNA delivery using capsule-mediated gastrointestinal tissue injections, Matter. 5 (2022) 975–987, https://doi.org/10.1016/j.matt.2021.12.022.
[28] A. Akinc, D.M. Lynn, D.G. Anderson, R. Langer, Parallel synthesis and biophysical characterization of a degradable polymer library for gene delivery, J. Am. Chem. Soc. 125 (2003) 5316–5323, https://doi.org/10.1021/ja034429c.
[29] A.K. Patel, J.C. Kaczmarek, S. Bose, K.J. Kauffman, F. Mir, M.W. Heartlein, F. DeRosa, R. Langer, D.G. Anderson, Inhaled nanoformulated mRNA polyplexes for protein production in lung epithelium, Adv. Mater. 31 (2019) 1–7, https://doi.org/10.1002/adma.201805116.
[30] Y. Li, Z. He, X. Wang, Z. Li, M. Johnson, R. Foley, A. Sigen, J. Lyu, W. Wang, Branch unit distribution matters for gene delivery, ACS Macro Lett. 12 (2023) 780–786, https://doi.org/10.1021/acsmacrolett.3c00152.
[31] Y. Liu, Y. Li, D. Keskin, L. Shi, Poly(β-amino esters): synthesis, formulations, and their biomedical applications, Adv. Healthc. Mater. 8 (2019) 1–24, https://doi.org/10.1002/adhm.201801359.
[32] D. Zhou, Y. Gao, A. Aied, L. Cutlar, O. Igoucheva, B. Newland, V. Alexeeve, U. Greiser, J. Uitto, W. Wang, Highly branched poly(β-amino ester)s for skin gene therapy, J. Control. Release 244 (2016) 336–346, https://doi.org/10.1016/j.jconrel.2016.06.014.
[33] M. Zeng, D. Zhou, F. Alshehri, I. Lara-Sáez, Y. Lyu, J. Creagh-Flynn, Q. Xu, A. Sigen, J. Zhang, W. Wang, Manipulation of transgene expression in fibroblast cells by a multifunctional linear-branched hybrid poly(β-amino ester) synthesized through an oligomer combination approach, Nano Lett. 19 (2019) 381–391, https://doi.org/10.1021/acs.nanolett.8b04098.
[34] D. Zhou, Y. Gao, J. O'Keeffe Ahern, A. Sigen, Q. Xu, X. Huang, U. Greiser, W. Wang, Development of branched poly(5-amino-1-pentanol-co-1,4-butanediol diacrylate) with high gene transfection potency across diverse cell types, ACS Appl. Mater. Interfaces 8 (2016) 34218–34226, https://doi.org/10.1021/acsami.6b12078.
[35] Y. Li, Z. He, J. Lyu, X. Wang, B. Qiu, I. Lara-Sáez, J. Zhang, M. Zeng, Q. Xu, A. Sigen, J.F. Curtin, W. Wang, Hyperbranched poly(β-amino ester)s (HPAEs) structure optimisation for enhanced gene delivery: non-ideal termination elimination, Nanomaterials 12 (2022) 3892, https://doi.org/10.3390/nano12213892.
[36] Z. Li, W. Ho, X. Bai, F. Li, Y. Jui Chen, X.Q. Zhang, X. Xu, Nanoparticle depots for controlled and sustained gene delivery, J. Control. Release 322 (2020) 622–631, https://doi.org/10.1016/j.jconrel.2020.03.021.
[37] P. Dosta, V. Ramos, S. Borrós, Stable and efficient generation of poly(β-amino ester)s for RNAi delivery, Mol. Syst. Des. Eng. 3 (2018) 677–689, https://doi.org/10.1039/c8me00006a.
[38] S.C. Hyde, I.A. Pringle, S. Abdullah, A.E. Lawton, L.A. Davies, A. Varathalingam, G. Nunez-Alonso, A.-M. Green, R.P. Bazzani, S.G. Sumner-Jones, M. Chan, H. Li, N. S. Yew, S.H. Cheng, A. Christopher Boyd, J.C. Davies, U. Griesenbach, D. J. Porteous, D.N. Sheppard, F.M. Munkonge, E.W.F.W. Alton, D.R. Gill, CpG-free plasmids confer reduced inflammation and sustained pulmonary gene expression, Nat. Biotechnol. 26 (2008) 549–551, https://doi.org/10.1038/nbt1399.